Journal of Electrical Engineering & Technology (2021) 16:141–153
https://doi.org/10.1007/s42835-020-00572-w

ORIGINAL ARTICLE

Improved Current Controlled Doubly Fed Induction Generator Model with Grid Integration Under Sub and Super Synchronous Conditions

Hamza Ahmad[1,2] · Hassan Khalid[3] · Arslan Ahmed Amin[4] · Neha Masroor[1,5] · Huda Mahmood[1] · Muhammad Abubakar[1]

Received: 25 April 2020 / Revised: 19 June 2020 / Accepted: 5 October 2020 / Published online: 2 November 2020

Abstract

This paper presents the development and experimental verification of the mathematical model of wind turbine and Doubly Fed Induction Generator (DFIG) using the current control and voltage estimation method between the DC link. The rotor of the induction generator (IG) is rotated with the wind turbine at a specific speed. The DFIG is directly coupled with a grid station and the synchronization between DFIG and the grid station is controlled by setting two converters: Machine Side Converter (MSC) implemented with the rotor side and Grid Side Converter (GSC) implemented with the grid. PI controllers have been utilized in the control loops and the parametric range is extracted to maximize the mechanical power transferred to the IG rotor. The model is tested under three conditions DFIG running at super synchronous speed, synchronous speed, and under synchronous speed using MATLAB Simulink. In the end, the same model is also tested through a series of experiments using lab modules. The results show that the proposed model is much simplified and accurate as compared to previous versions available in the literature.

Keywords DFIG modelling · Induction generator · Wind turbine · Grid side converter · Machine side converter

List of Symbols

A	Turbine swept area
β	Blade Pitch angle
ψ_r	Rotor side flux
ψ_s	Stator side Flux
C_P	Performance factor
C_p	Power coefficient
DFIG	Doubly fed induction generator
DSL	Dynamic simulation language
E_{wind}	Wind energy
GSC	Grid Side converter
H	Motor inertia
IG	Induction generator
i_s	Stator current
i_r	Rotor current
I_{abc}	Three phase line current
L_m	Mutual inductance
L_r	Rotor side inductance
L_s	Stator side inductance
λ	Tip speed ratio
P_g	Grid active power
P	Number of poles
P_m	Mechanical power
Q_g	Grid reactive power
R_r	Rotor resistance
R_s	Stator resistance
T_e	Induced torque

✉ Arslan Ahmed Amin
arslan_engineer61@yahoo.com

Hamza Ahmad
hamza4524@gmail.com

Hassan Khalid
Khalid.hassan18@yahoo.com

[1] Department of Electrical Engineering, Pakistan Institute of Engineering and Applied Sciences (PIEAS), Islamabad, Pakistan

[2] School of Electrical and Electronics Engineering, Chung-Ang University, Seoul, South Korea

[3] Department of Electrical Engineering, NFC Institute of Engineering and Technology, Multan 59060, Punjab, Pakistan

[4] Department of Electrical Engineering, FAST National University of Computer and Emerging Sciences, Chiniot Faisalabad Campus, Lahore 35400, Punjab, Pakistan

[5] Department of Energy Systems Engineering, UPCASE, National University of Science and Technology (NUST), Islamabad, Pakistan

T_m	Mechanical torque
V_{DC}	DC voltage
V_{abc}	Three phase line voltage
V_r	Rotor side voltage
V_s	Stator side voltage
V_{wind}	Wind velocity
θ_e	Synchronously rotating angle
ω_r	Rotor angular velocity (rev/min)
ω_s	Synchronous speed (rev/min
MSC	Machine side converter
NREL	National Renewable Energy Laboratory
t	Time
THD	Total harmonic distortion

1 Introduction

It has been estimated that power generation through wind will reach 300 GW until 2020, which is 20% of the whole energy production [1] The increasing demand for energy by society leads to scarcity of natural resources like coal, natural gas and oil [2] Renewable energy resources including wind, solar and dams are considered as everlasting forms of energy extraction methods but each method has certain limitations. However, wind energy and hydropower stations have many things in common and both of them can be synchronized together to get even a high amount of power.

While considering wind energy as a renewable energy source, the induction generator (IG) becomes really important. The conventional power plants utilize synchronous generator as they operate at synchronous speed and consumes high cost to regulate their speed by using a prime mover, mostly diesel engines and are the least cost-effective than induction machines. On the other hand, IG which is mostly self-exited can operate on variable speed even higher than synchronous speed [3] and are mostly suitable when connected by wind turbines.

The wind gyrators units use fixed and variable speed turbines [5], despite varying wind variable wind generators are opted to capture maximum power. Among all the variable speed generators double-fed generators (DFIG) coupled with the rotor side, power converters are now commonly available. Recently, the control of high performing induction machines has gained a lot of attention from industrial applications. The wind generator manufacturing companies are required to provide descriptive simulation model for their product [6]. Since this information is confidential and vendors do not provide such information, therefore, the mathematical modeling of such machines has attracted researches a lot in predicting the load characteristics and this is mainly due to the varying modes of operation including both steady-state and dynamic state [7, 8]. Much of the work has been done in simplifying the model, the impact of DFIG model simplicity was of main concern and the model stability was analyzed by neglecting resistance of rotor and stator [9].

The WTG model thus developed were validated by [10] and it showed the importance of distributed modeling in wind farm through IEC 61400-27 standard. Field-based measurement, the IEC Type-3 model for wind turbines based on voltage controller and wind power factor controller is verified in [11].

Although the current control based model has widely been used for DFIG modeling, but the model validation in previous works is carried out by using step input reference. However, it requires intensive analysis for various conditions when DFIG is connected to the grid under various modes. The IEC/WECC Type-3 WTG model is one of the benchmarks of the current–source model. The simulation-based DFIG model and its applications are described in [12] but still, it lacks the analysis.

In this paper, our contribution is to present the mathematical model analysis of wind turbines connected with the current control IG which is synchronized with the power grid station by implementing the DFIG controller to power electronics converters serving between the grid side and rotor side of IG. The power electronics converter model between the grid and the DFIG is based on the current control loop that monitors the speed of the wind turbine and its control through the current control strategy instead of just stepped input. The model of DFIG and its synchronization with the grid is also investigated through the synchronization of GSC and MSC and the back and forth power transfer in sub to synchronous and super synchronous operation in along with lab experiment.

This paper will be organized as follows. In Sect. 1 a brief history has been presented for the related work done on DFIG, Sect. 2 presents the mathematical model of wind turbine and suggests parameters for obtaining maximum mechanical power from a wind turbine and implements the mathematical model of DFIG, Sect. 3 presents the converter modeling strategy, Sects. 4 and 5 presents grid and machine side converters, Sect. 6 the simulation and experimental results for our proposed scheme and Sect. 7 concludes the whole discussion.

2 Wind Turbine Modeling and Integration with DFIG

The wind turbine shown in Fig. 1 is directly coupled with the rotor of the IG. The wind turbine extracts wind energy from the swept area of the rotor and transforms it into electrical energy. The mechanical power (P_m) delivered by the wind turbine is given by the following Eq. [13]

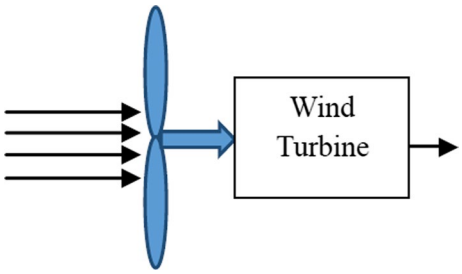

Fig. 1. Windmill connected to wind turbine

$$P_{wind} = \frac{1}{2} A \rho C_p {V_{wind}}^3, \tag{1}$$

where (C_p) is known as the coefficient of power, (A) is the turbine's blade swept area (m^2), (ρ) is the air density (kg/m^3) and $\left(V_{wind}\right)$ is the velocity of the wind in (m/s).

The energy delivered by the turbine towards the IG rotor is given by the following Eq. [14]

$$E_{wind} = P_m \times t. \tag{2}$$

During power transformation, not all the power is delivered by the wind to the rotor. Since the energy remains conserved, therefore, using Betz theorem [14] the mechanical power can be obtained using the performance power coefficient ratio and is given by the following equation

$$C_p = \frac{P_m}{P_{wind}}. \tag{3}$$

In Eq. (1) C_p is not a constant but is a two-dimension dependent state function. One parameter is known as fractional tip speed (λ) and other one is blade pitch angle (β) and is expressed by using the following equation

$$\lambda = \frac{\omega_r R}{V_{wind}}. \tag{4}$$

Here, ω_r is the angular velocity (rev/min) of the turbine rotor and is controlled by using gearbox. The mechanical torque induced (T_m) by the wind turbine during rotation is given by the following Eq. (6) where (C_T) is termed as the torque coefficient and is given by Eq. (7)

$$P_m = T_m \omega_r, \tag{5}$$

$$T_m = \frac{1}{2} A R \rho C_T {V_{wind}}^2, \tag{6}$$

$$C_T = \frac{C_P}{\lambda}. \tag{7}$$

The state variables of power coefficient for VSWT [15] can be summarized by the following equation

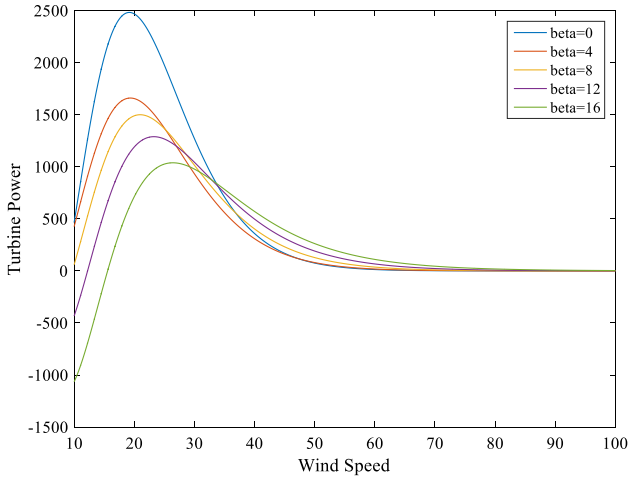

Fig. 2 The turbine power delivered as a function of wind speed for different blade angles

$$C_p(\lambda, \beta) = 0.73\left[\frac{151}{\lambda_i} - 0.58\beta - 0.002\beta^{2.14} - 13.2\right] e^{18.4/\lambda_i}. \tag{8}$$

The mechanical power obtained from the wind turbine as a function of wind speed at various blade pitch angles is shown in Fig. 2. Similarly, the performance coefficient of the wind turbine termed as implicit function of the speed tip ratio is demonstrated in Fig. 3. The output characteristics curves in Fig. 2 reveal that in the beginning the output power drastically rises as the level of wind increases but then significantly drops to zero and the amplitude of turbine power also declines by increasing the pitch angle of blades. Similarly, the performance factor (C_P) at first

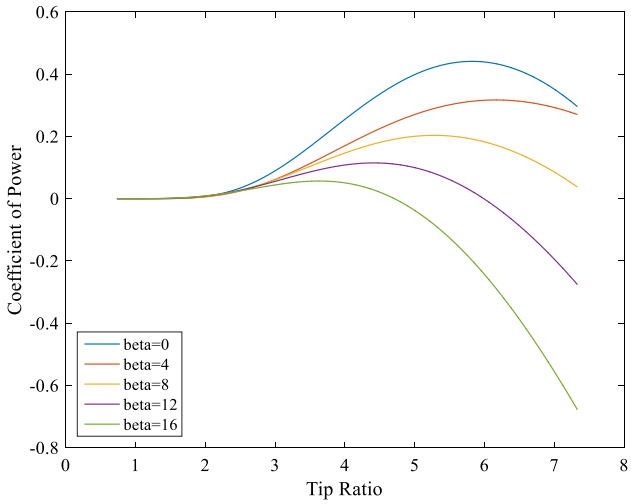

Fig. 3 Performance coefficient factor as a function of the speed tip ratio for different blade angles

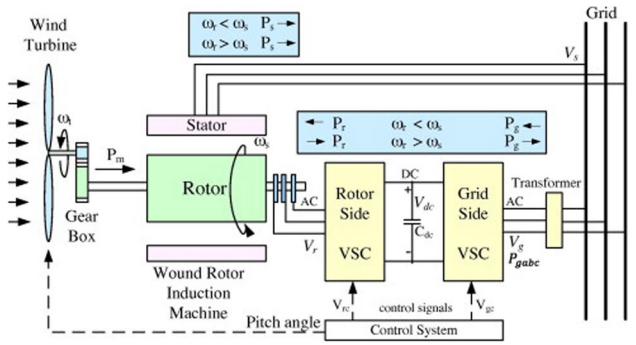

Fig. 4 Integration of DFIG with wind turbine

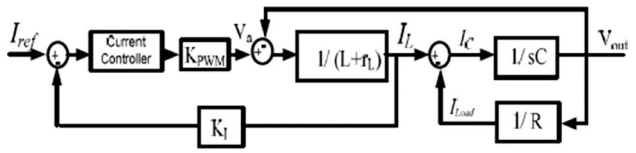

Fig. 5 The control scheme for MSC

increases but then starts to decline as the tip ratio crosses its knee value as shown in Fig. 3.

The adopted model of DFIG is an analytical model of the following equations and the basic configuration is shown in Fig. 4 [14]. Where the induction machine works as a motor when the rotor angular velocity is less than synchronous velocity and works as a generator when the rotor angular velocity is greater than the synchronous velocity. The three-phase induction machine can be translated into a two axis synchronously rotating frame of reference using Clark and Park transformation theorems. The resulting frame of reference corresponds dynamic quadrature d-q with (θ_e) synchronously rotating angle [13, 16]. Using the basic model of squirrel cage wound rotor type induction motor as shown in Fig. 5 can be modified to operate it as an induction generator at variable speed and the equations in a d-q model for stator and rotor sides are lined as follows.

The stator and rotor circuit equations (referred to stator) in the stationary frame of reference become:

$$V_s^s = R_s i_s^s + \frac{d\psi_s^s}{dt}, \tag{9}$$

$$V_r^s = R_r i_r^s + \frac{d\psi_r^s}{dt}. \tag{10}$$

The d-q transformed stator circuit equations in a synchronously rotating frame of reference are:

$$V_{qs} = R_s i_{qs} + \frac{d\psi_{qs}}{dt} + \omega_s \psi_{qs}, \tag{11}$$

$$V_{ds} = R_s i_{ds} + \frac{d\psi_{ds}}{dt} - \omega_s \psi_{ds}. \tag{12}$$

Similarly, rotor circuit equations turn out to be:

$$V_{qr} = R_s i_{qr} + \frac{d\psi_{qr}}{dt} + (\omega_s - \omega_r)\psi_{qr}, \tag{13}$$

$$V_{dr} = R_s i_{dr} + \frac{d\psi_{dr}}{dt} - (\omega_s - \omega_{r)}\psi_{dr}. \tag{14}$$

Flux linkages in terms of currents are given by:

$$\psi_{qs} = L_s i_{qs} + L_m i_{qr} = L_{Is} i_{qs} + L_m\left(i_{qs} + i_{qr}\right), \tag{15}$$

$$\psi_{ds} = L_s i_{ds} + L_m i_{dr} = L_{Is} i_{ds} + L_m\left(i_{ds} + i_{dr}\right), \tag{16}$$

$$\psi_{qr} = L_r i_{qr} + L_m i_{qs} = L_{Ir} i_{qr} + L_m\left(i_{qs} + i_{qr}\right), \tag{17}$$

$$\psi_d r = L_r i_d r + L_m i_d s = L_I r i_d r + L_m (i_d s + i_d r) \tag{18}$$

$$\psi_{qm} = L_m\left(i_{qs} + i_{qr}\right), \tag{19}$$

$$\psi_{dm} = L_m\left(i_{ds} + i_{dr}\right). \tag{20}$$

The electromechanical torque is given by

$$T_e = \left(\frac{3}{2}\right)\left(\frac{P}{2}\right)\left(\psi_{ds} i_{qs} - \psi_{qs} i_{ds}\right), \tag{21}$$

where (P) is the number of poles of the induction machine.

$$\frac{d\left(w_r/w_b\right)}{dt} = \frac{1}{2H}\left(T_e - T_m\right), \tag{22}$$

where (H) is the inertia constant (w_b) is the base frequency and T_m is the machine induced torque. In order to make it work as a generator rotor is rotated using a wind turbine, this creates a reverse torque, and the power of the generator increase. Since there is a limitation because of a lack of field excitation, reactive power is supplied by connecting reactive load like a capacitor at the stator side.

3 Converter Modeling

The basic structure of DFIG consists of only two main controllers which are employed in Grid Side Converter (GSC) and Machine Side Converter (MSC). The GSC controller

controls the DC link voltage and power exchange with the grid while the MSC controller controls the power of the stator. A classical vector control method is used in this work to control the DFIG [17]. DC link voltage is estimated by using the following equation [18, 19].

$$\mathbf{V_{DC}} \geq \frac{2\sqrt{2}}{\sqrt{3}\mathbf{m}}\mathbf{V_{ab}}. \tag{23}$$

4 Machine Side Converter (MSC)

The MSC is designed by a vector control method using the stator flux scheme shown in Fig. 5. The d-axis is in alignment with the stator flux. There's a linear relationship between stator flux and grid voltage. If we neglect the small voltage drop caused by stator resistance, we get:

$$V_{qs} = V_g \approx \omega_s \psi_s. \tag{24}$$

This results in the following equations

$$\boldsymbol{\psi_{qs}} = \boldsymbol{L_s i_{qs}} + \boldsymbol{L_m i_{qr}} = 0, \tag{25}$$

$$\boldsymbol{\psi_{ds}} = \boldsymbol{L_s i_{ds}} + \boldsymbol{L_m i_{dr}} = \boldsymbol{\psi_s}. \tag{26}$$

From the above equations, we can calculate the d-q axis stator currents

$$\mathrm{i_{qs}} = -\frac{\mathrm{L_m}}{\mathrm{L_s}}\,\mathrm{i_{qr}}, \tag{27}$$

$$i_{ds} = \frac{\psi_s - L_m}{L_s} i_{dr}. \tag{28}$$

Substituting the values of i_{qs} and i_{ds} in $\mathrm{P_s}$ and $\mathrm{Q_s}$, we get

$$i_{qr} = -\frac{2L_s}{3V_g L_s} P_s, \tag{29}$$

$$i_{dr} = -\frac{2\mathrm{Q_s} L_m}{3V_g L_s} Q_s. \tag{30}$$

The above-mentioned rotor dynamic and quadrature currents serve as a current controlling model of IG.

The PWM converter is employed on the rotor and the control is done by PWM signals, the stator and rotor current, and the position of the rotor [20].

The MSC converter controller can be designed using stator flux control. There are two cascaded control loops of the MSC control scheme. The *d*-axis and *q*-axis rotor current components are regulated independently by the inner current control loop with respect to some synchronously rotating reference frames [17].

The inner current control loop can be designed using the Eqs. (12) and (13). A Proportional and Integral (PI) controller is designed for this purpose. The proportional and integral gain is decided using these equations.

$$\boldsymbol{v_{dr}} = (\boldsymbol{k_p} + \frac{\boldsymbol{k_i}}{\boldsymbol{s}})(\boldsymbol{i_{dr}^*} - \boldsymbol{i_{dr}}) - \boldsymbol{s\omega_r \sigma L_r i_{qr}}, \tag{31}$$

$$\boldsymbol{v_{qr}} = (\boldsymbol{k_p} + \frac{\boldsymbol{k_i}}{\boldsymbol{s}})\left(\boldsymbol{i_{qr}^*} - \boldsymbol{i_{qr}}\right) + \boldsymbol{s\omega_r(\sigma L_r i_{dr})} + \frac{\boldsymbol{L_m}^2}{\boldsymbol{L_s}}\boldsymbol{i_{ms}}, \tag{32}$$

where σ is given by

$$\boldsymbol{\sigma} = 1 - \frac{\boldsymbol{L_m}^2}{\boldsymbol{L_s L_r}}. \tag{32}$$

The gains of the PI controller have been tuned using Ziegler Nichols method [21] followed by experimental fine tuning and are mentioned in Table 1.

5 Grid Side Converter (GSC)

The power of the grid is used to model the current loops that control the IGBTs using PI controllers. The active power components give the reference grid current of the dynamic axis, while the reactive power gives the grid current of the quadrature axis as in Eq. (33) to (36). The required vector control strategy is accomplished by aligning the dynamic axis of the synchronous frame with the vector of grid voltage.

$$P_g = \frac{3}{2}\left(V_{dg} i_{dg} + V_{qg} i_{qg}\right) = \frac{3}{2} V_{dg} i_{dg}, \tag{33}$$

$$Q_g = \frac{3}{2}\left(V_{qg} i_{dg} - V_{dg} i_{qg}\right) = -\frac{3}{2} V_{dg} i_{qg}, \tag{34}$$

$$i_{dg}^* = \frac{2P_g^*}{3V_{dg}}, \tag{35}$$

$$i_{qg}^* = -\frac{2Q_g^*}{3V_{dg}}. \tag{36}$$

Table 1 Parameters for PI controller

Gain	Value
$\mathrm{K_p}$	0.07
$\mathrm{K_i}$	10

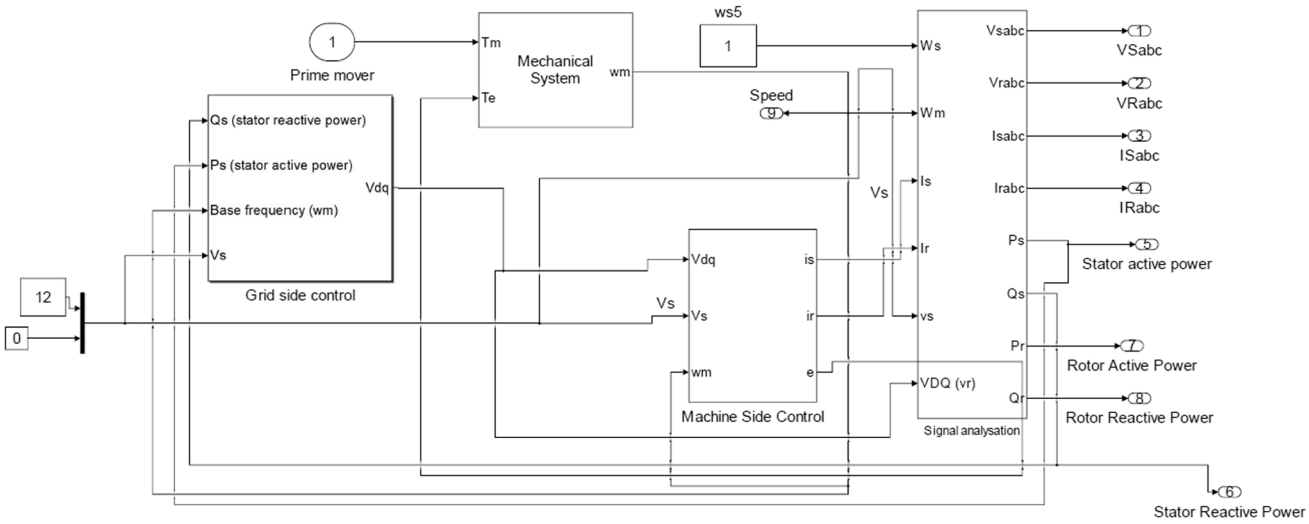

Fig. 6 The vector control diagram of the GSC mode

The three-phase line voltage (V_{abc}) and current (I_{abc}) are used to estimate the stator fluxes. The rotating angle of the rotor is obtained from DFIG and then the a-b-c model is transformed into a d-q model where all the rotating currents are obtained using PI controllers. Finally, rotor d-q voltages are accomplished as stated in Eq. (31) and (32), these switching voltages are used to generate PWM signals that control switching of IGBTs as shown in Fig. 6

$$V_{af} = R_f i_{ag} + \frac{di_{ag}}{dt} L_f + V_{ag}, \tag{37}$$

$$V_{bf} = R_f i_{bg} + \frac{di_{bg}}{dt} L_f + V_{bg}, \tag{38}$$

$$V_{cf} = R_f i_{cg} + \frac{di_{cg}}{dt} L_f + V_{cg}. \tag{39}$$

6 Results and Discussions

This section completely illustrates the DFIG model implementation and its operation through simulation results. The model is developed to test under three conditions i.e. sub-synchronous speed, synchronous speed, and super synchronous speed. The reactive and active power impacts on rotor speeds by connecting capacitor is observed against grid and machine side converters through voltages.

For DFIG to work in super-synchronous mode, the rotor angular frequency is much higher as compared to the stator angular frequency. Initially the value of slip is assumed to be zero and the turbine supply two times of the p.u torque

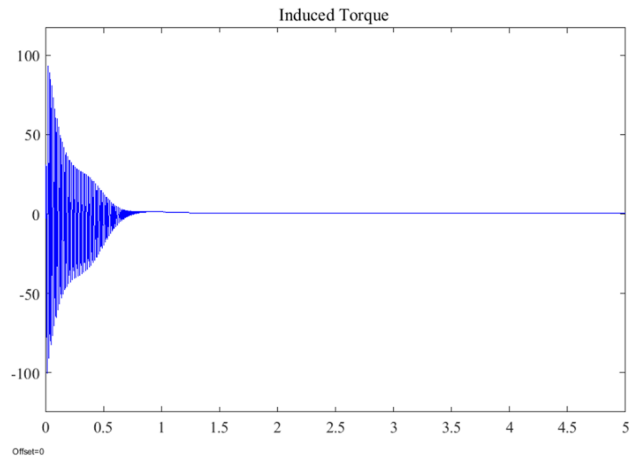

Fig. 7 Torque induced by machine running in super synchronous model

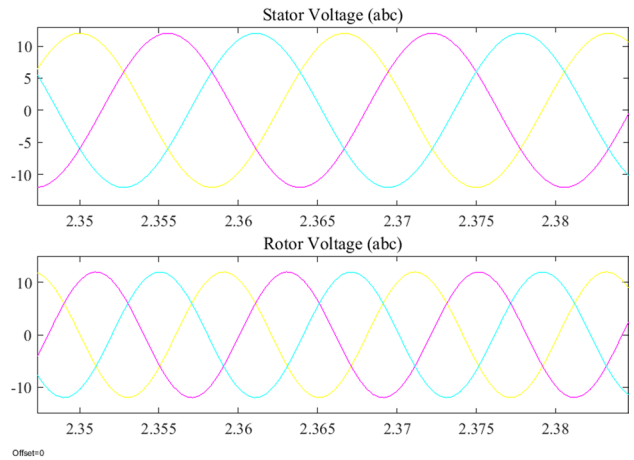

Fig. 8 Three phase stator and rotor voltage induced in super synchronous model

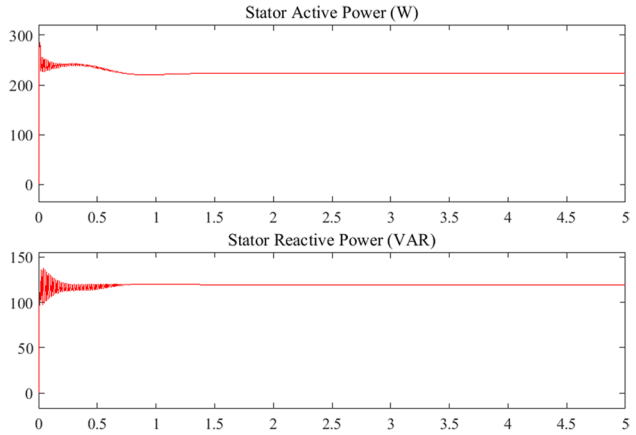

Fig. 9 Stator active and reactive power during super synchronous model

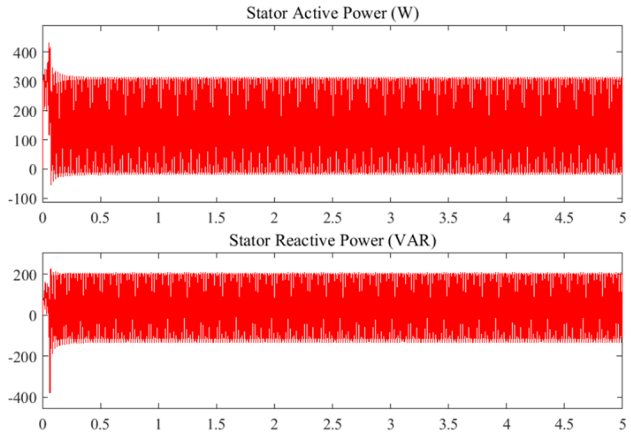

Fig. 11 Stator side active and reactive power running in synchronous mode

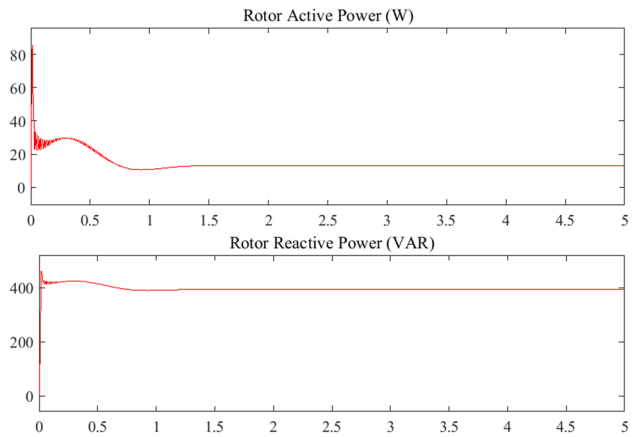

Fig. 10 Rotor active and reactive power in super synchronous model

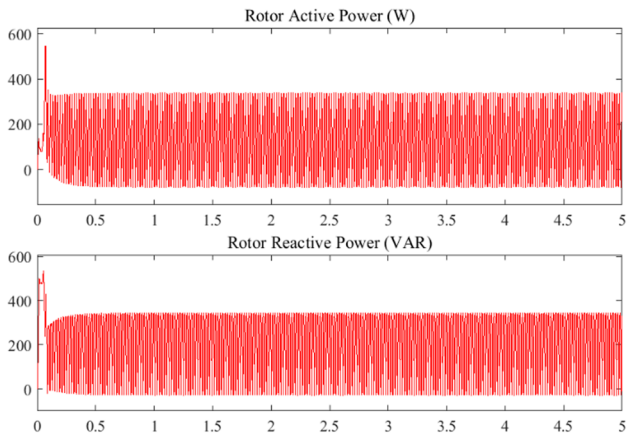

Fig. 12 Rotor side power consumed in synchronous mode

to the rotor and thus the positive torque induces the voltage across the stator. The torque induced by the machine is shown in Fig. 7. It can be clearly seen that the torque induced is positive. The induced stator and rotor voltages are shown in Fig. 8. The waveform of induced stator three phase voltage frequency is found to be less as compared to the frequency of rotor. This implies that power is fed to the grid side. This clearly illustrates that slip has become negative and the machine is acting as generator. The active and reactive power consumed by the stator and rotor are shown in Figs. 9 and 10. It is clear that rotor active power consumed is almost negligible and reactive power consumed is due to reactive element connected at stator side.

In synchronous mode, the rotor and stator frequency becomes equalized and in this way, the slip approaches to zero. In this mode, no power is transferred to the grid side by the induction generator. In this way, the active component of the rotor becomes zero however, the reactive

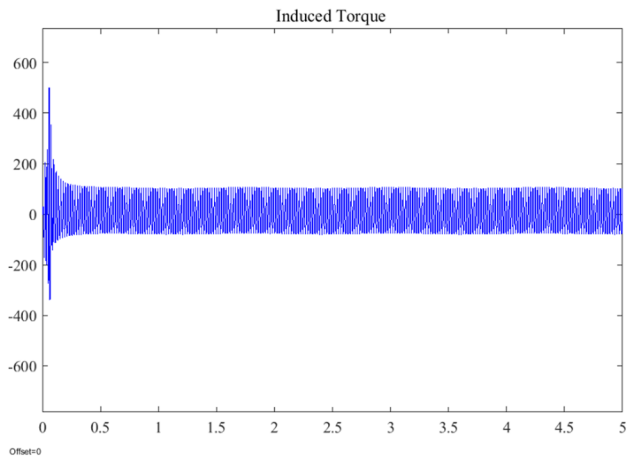

Fig. 13 Torque induced in synchronous mode

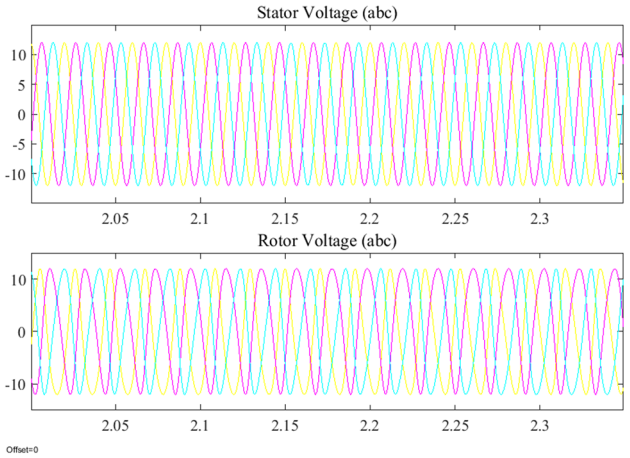

Fig. 14 Three phase statot and rotor voltage induced in synchronous model

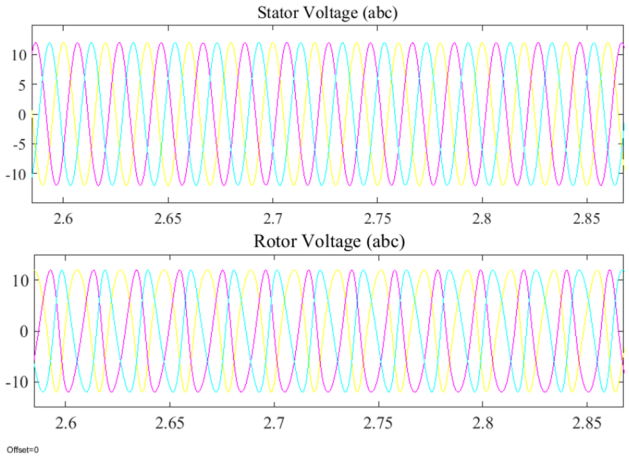

Fig. 16 Thre phase stator and rotor voltage in sub-synchronous mode

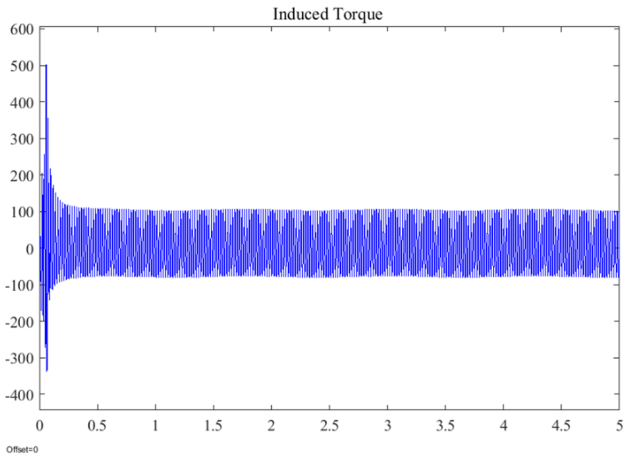

Fig. 15 Torque induced in sub-synchronous mode

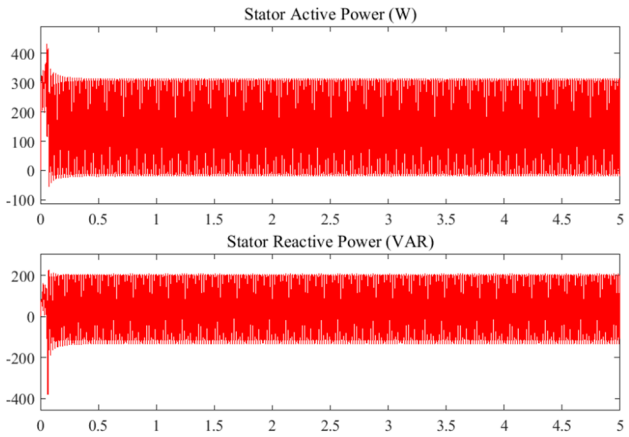

Fig. 17 Stator side active and reactive power in sub-synchronous mode

power of the rotor will exist due to the reactive element connected by the stator as shown in Figs. 11 and 12. The induced torque in Fig. 13 shows that the induction machine is baring the load and at this stage the power is not delived to the grid side and nor we can say that the machine is totally running in motoring mode. The three phase rotor and stator side voltages induced are shown in Fig. 14. The system is highly stable due to frequency synchronization.

In the third condition, the double fed induction generator is made to run in sub synchronous mode. For this purpose, the stator frequency will be more than that of rotor frequency. In this way, the DFIG will run below the synchronous speed and the rotor will not be able to transfer power towards the grid. This will cause the slip to be lesser than one and greater than zero, now the power from the grid will be consumed by the rotor. The DFIG running lesser than synchronous speed draws power from the grid side towards the rotor and now the rotor consumes both active and reactive power from the grid side. The torque induced by the IG is shown in Fig. 15 and it can be clearly seen that motor is bearing a load and its torque will be positive, the three phase voltage induced waveforms of stator and rotor clearly indicate that the frequency of rotor is less than the stator side frequency as in Fig. 16. Since the power is consumed by the motor therefore, the both active and reactive power component will be cosumed by both rotor and stator winding as shown in Figs. 17 and 18.

The above simulation model was also tested by setting the testing bed in the lab and Labsoft was used to establish the wind farm emulator. The experimental setup prepared is shown in Fig. 19 The modern wind systems employ DFIG for variable wind speed control and ensure optimum energy transfer. The experimental setup consists of thirty-seven units and the list is presented in Table 2. The first test performed shows the dependency of mechanical rotating speed

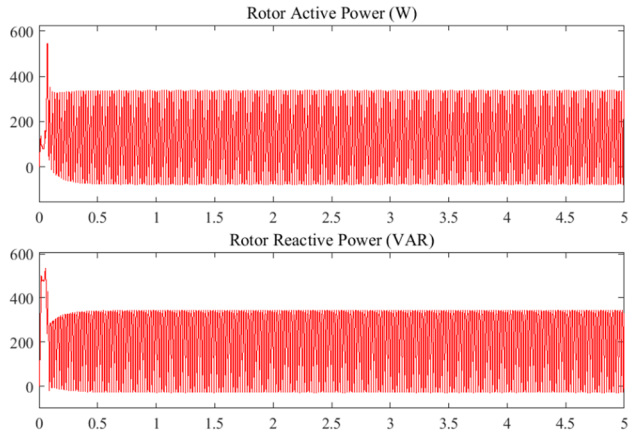

Fig. 18 Rotor side active and reactive power in sub-synchronous mode

over the generated supply frequency. The statistical data in Table 3 shows that the DFIG behaved as the synchronous generator over the variable mechanical speed range with a wide range of frequencies. The next test performed reveals the influence of variable frequency rotor and the following conclusions were made (i) the stator frequency could be held constant by adjusting rotor frequency for certain mechanical delivered speed by the wind turbine. (ii) At constant speed the stator frequency can be varied via rotor frequency and (iii) Stator speed is the sum of rotor frequency and the frequency of mechanical rotating wind turbine. the results have been summarized in Table 4.

The results obtained from Tables 3 and 4 help to formulate a relationship to understand the impact of changing rotor frequency at a certain rotor current over the per phase stator voltage. The results presented in Table 5 help to conclude that by increasing the rotor frequency by just 10 Hz will increase the stator voltage at 50 Hz proportionally. Also by increasing the rotor current for the same rotor frequency will also increase the induced stator voltage per phase. The results for the influence of rotor current over stator voltage at different levels of rotor frequency have been summarized in Table 5.

In order to control power through DFIG, its power is varied under sub-synchronous mode. This mode power required to excite the generator is received from the grid and in this mode power is fed to the DFIG. And the results have been demonstrated in Fig. 20 The power through generator can also be controlled by speed variation of generator. The results for speed variation of generator for fixed power supplied by IG at 400 W can be controlled and fed to grid side is shown in Fig. 21. The GSC power will steady rise due to large consumption of reactive power. Similarly, the power can be controlled in super synchronous mode for both which means that now the rotor frequency is higher than stator frequency, this means that power is being fed to the grid side through MSC and GSC. In this case the DFIG power is steadily raised and the reactivein power of GSC will steadily decrease. The experimental result has been shown in Fig. 22.

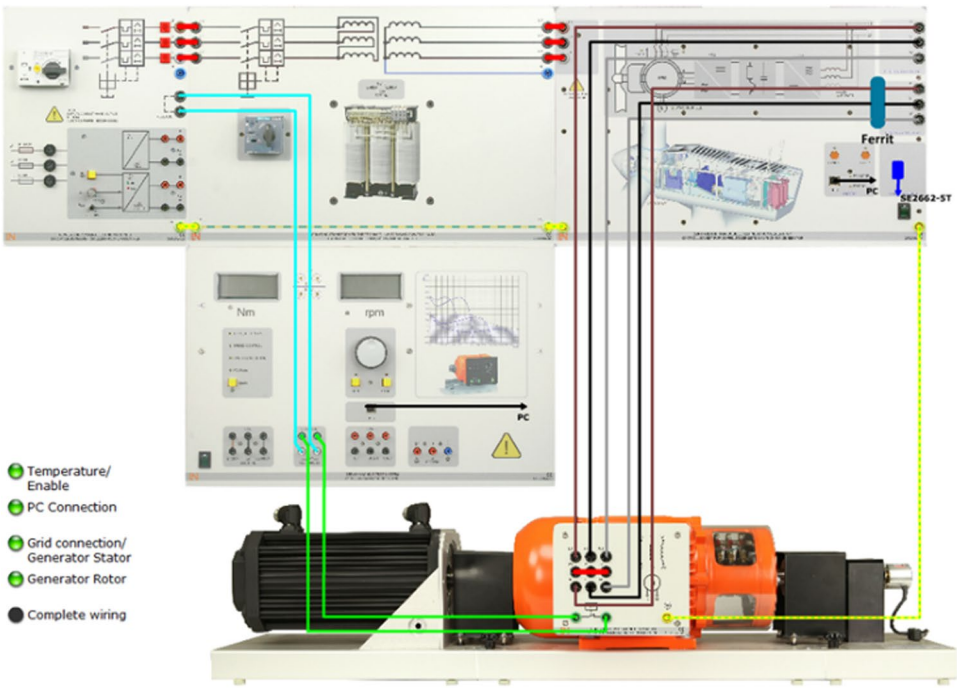

Fig. 19 The experimental setup of Grid-connected DFIG

Table 2 Equipment used to connect DFIG to Grid

Equipment code	Description	Number of units
CO3208-3A	Controller for wind power plant DFIG	1
CO3208-3B	Three-phase isolating transformer for wind power plant	1
SE2662-6 W	Three-phase, multi-function machine (double fed generator)	1
SE2662-5 T	Incremental position encoder (1024 pulses)	1
CO3636-6 W/CO2663-6U	Servo machine test stand (1 kW)	1
SE2662-6A	Coupling sleeve (1 kW)	2
SE2667-6B	Coupling guard (1 kW)	2
CO5127-1Z	Analog/digital multimeter	1
SO5148-1L	Set of safety connecting cables (4 mm)	1
SO5126-9Y	Safety connecting plugs (4 mm)	20
So5126-9R	Safety connection plug (19/4 mm) with tap	5

Table 3 Mechanical speed influence over DFIG in synchronous mode

Mechanical Speed (rpm)	1200	1300	1400
Mechanical frequency (Hz)	40	44	47
Voltage frequency (Hz)	40	44	47

Table 4 Mechanical speed influence over DFIG in for variable rotor frequency (sub-synchronous mode)

Mechanical Speed (rpm)	1200	1300	1400
Voltage frequency (Hz)	10	7	3
Stator frequency (Hz)	50	50	50

7 Conclusion

This paper presented the implementation of an analytical model of DFIG connected with wind turbines and its integration with the grid using current control loops. The implemented mathematical model was tested under synchronous, subsynchronous and super synchronous mode and the results obtained were briefly discussed in the above section. The results revealed that when the rotor is rotating at an angular

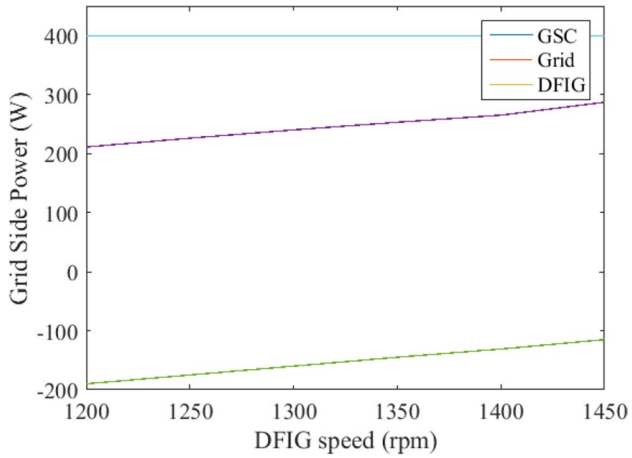

Fig. 21 Power control by DFIG running in subsynchronous mode at veriable speed

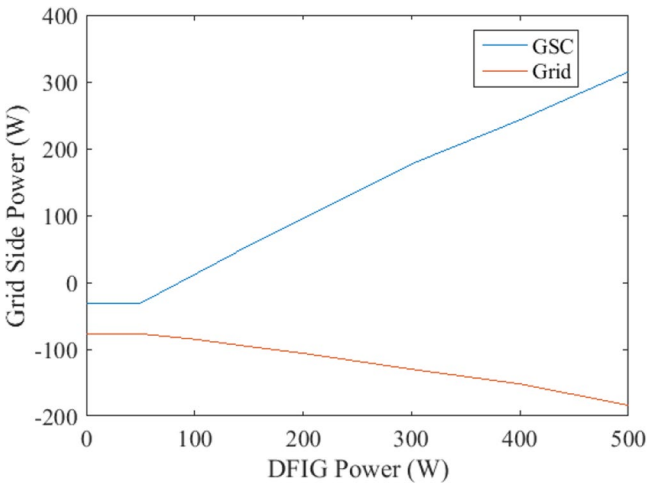

Fig. 20 Power control by DFIG running in subsynchronous mode at variable power supplied by GSC

Table 5 Stator voltage at different levels of rotor frequency for variable rotor current

Variable rotor frequency	I rotor (A)	0.5	1	1.5	2	2.5	3
Rotor frequency = 0 Hz	U stator (V)	62	115	189	225	270	295
Rotor frequency = 10 Hz	U stator (V)	70	155	225	290	330	350

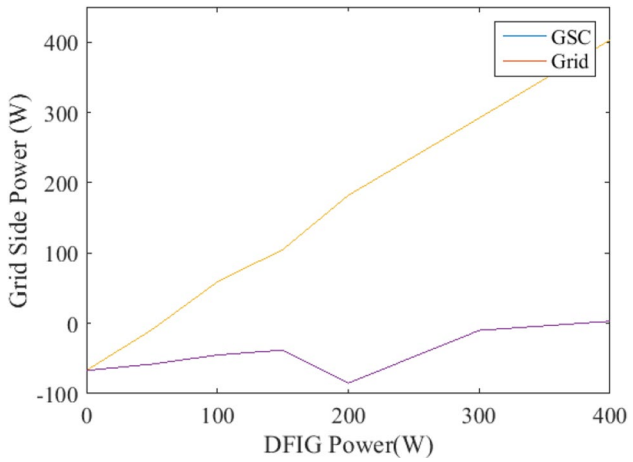

Fig. 22 Power fed to grid by DFIG in super synchronous mode

frequency lower than the stator angular frequency then the power is fed to the rotor from grid side and when the angular frequency of rotor is higher than the stator angular frequency, the power is fed to the grid from rotor side. The mathematical model was also tested under the lab integrating the DFIG model with the grid under the same conditions and the results thus obtained completely validated our model. Further tests have been performed to analyze the change of rotor current and frequency over stator induced voltage. It showed that under sub synchronous mode the reactive power from GSC continuously increases in negative. However, in super-synchronous mode, the reactive power of GSC becomes positive due to a decrease in reactive power. The lab experiment has also been validated by running DFIG at variable and fixed speed to show the variation of power transfer from the grid to DFIG and toward the grid.

Acknowledgements The authors would like to thank to colleagues for suggestions to improve the paper quality.

References

1. U. S. E. (2013) Supply, 20% wind energy by 2030. Increasing wind energy's contribution TO U.S. electricity supply. Wind power: technology, economics and policies, pp 99–333. GO-102008–2567.
2. Luiz Lacerda Ferreira Murari A, Alberto Torrico Altuna J, Vani Jacomini R, Mario Rocha Osorio C, Sebastian Solis Chaves J, Joaozinho Sgaurezi Filho A (2017) A Proposal of Project of PI controller gains used on the Control of Doubly-Fed Induction Generators. In: IEEE Latin America Transactions, vol. 15, no. 2, pp 173–180. https://doi.org/10.1109/TLA.2017.7854609
3. Meshcheryakov VN, Muravyev AA, Boikov AI (2018) Induction generator based on doubly-fed machine. In: 2018 17th International Ural Conference on AC Electric Drives (ACED), no. 1, pp 1–5. https://doi.org/10.1109/ACED.2018.8341719
4. Sousa GCD, Martins FN, Sousa GCD, Martins FN (2015) An autonomous fuzzy controlled induction generator system with voltage regulation velocity-based dynamic model and adaptive controller for differential steered mobile robot view project optimizing robot controller gains with Genetic Algorithm View project, 2004. https://doi.org/10.13140/RG.2.1.4837.2328
5. Müller S, Deicke M, De Doncker RW (2002) Doubly fed induction generator systems for wind turbines. IEEE Ind Appl Mag 8(3):26–33. https://doi.org/10.1109/2943.999610
6. Ma J, Zhao D, Yao L, Qian M, Yamashita K, Zhu L (2018) Analysis on application of a current-source based DFIG wind generator model. CSEE Journal of Power and Energy Systems 4(3):352–361. https://doi.org/10.17775/cseejpes.2018.00060
7. Asgari SH, Jannati M, Idris NRN (2014) Modeling of three-phase induction motor with two stator phases open-circuit. In: 2014 IEEE Conference on Energy Conversion (CENCON), pp 231–236, https://doi.org/10.1109/CENCON.2014.6967507
8. Shah S, Rashid A, Bhatti MKL (2012) Direct quadrate (d-q) modeling of 3-phase induction motor using matlab/simulink. Can J Electr Electron Eng 3(5):237–243
9. Zhang D, Wang Y, Hu J, Ma S, He Q, Guo Q (2016) Impacts of PLL on the DFIG-based WTG's electromechanical response under transient conditions: analysis and modeling. CSEE J Power Energy Syst 2(2):30–39. https://doi.org/10.17775/cseejpes.2016.00019
10. Zhang Y, Muljadi E, Kosterev D, Singh M (2015) Wind power plant model validation using synchrophasor measurements at the point of interconnection. IEEE Trans Sustain Energy 6(3):984–992. https://doi.org/10.1109/TSTE.2014.2343794
11. Goksu O, Altin M, Fortmann J, Sorensen PE (2016) Field validation of IEC 61400–27-1 wind generation type 3 model with plant power factor controller. IEEE Trans Energy Convers 31(3):1170–1178. https://doi.org/10.1109/TEC.2016.2540006
12. V. W. Group (2015) Value and limitations of the positive sequence generic models of 2.0. The value of the generic model structures
13. Xu M, Gu T, Xu J, Wang K, Li G, Guo F (2018) Electromechanical modeling of the direct-driven wind turbine generator considering the stochastic component of wind speed. In: 2018 2nd IEEE Conference on Energy Internet and Energy System Integration (EI2), no. 1, pp 1–4. https://doi.org/10.1109/EI2.2018.8582114
14. Dadhania A, Venkatesh B, Nassif AB, Sood VK Modeling of doubly fed induction generators for distribution system power flow analysis. Int J Electr Power Energy Syst 53(1):576–583. https://doi.org/10.1016/j.ijepes.2013.05.025
15. Khajuria S, Kaur J (2012) Implementation of pitch control of wind turbine using simulink (Matlab), vol. 1, no. 4, pp 196–200
16. Ong C-M (1998) Dynamic simulation of electric machinery, 1st edn. Prentice Hall, London, pp 141–155
17. Berhanu Tuka M, Leidhold R, Mamo M (2017) Modeling and control of a doubly fed induction generator using a back-to-back converters in grid tied wind power system. In: 2017 IEEE PES

PowerAfrica, pp 75–80. https://doi.org/10.1109/PowerAfrica.2017.7991202
18. Swami Naidu NK, Singh B (2015) Doubly fed induction generator for wind energy conversion systems with integrated active filter capabilities. In: IEEE transactions on industrial informatics, vol. 11, no. 4, pp 923–933. https://doi.org/10.1109/TII.2015.2446767
19. Sharma S, Singh B (2011) Voltage and frequency control of asynchronous generator for stand-alone wind power generation. IET Power Electron 4(7):816. https://doi.org/10.1049/iet-pel.2011.0007
20. Li S, Haskew TA (2007) Analysis of decoupled d-q vector control in DFIG back-to-back PWM converter. In: 2007 IEEE power engineering society general meeting, pp. 1–7. https://doi.org/10.1109/PES.2007.385461
21. Hughes TA (2015) Measurement and control basics. In: Measurement and control basics, 5th ed., International Society Automation, p. 409

Hamza Ahmad received the B.S. degree in Electrical Engineering from Pakistan Institute of Engineering and Applied Sciences (PIEAS), Pakistan, in 2018. He is currently pursuing his MS degree as a Graduate Research Assistant at Chung-Ang University, Seoul, South Korea. His research interests include design and optimization of electrical machines and Applications of smart electromagnetic Smart materials.

Hassan Khalid has received his B.Sc. in Electrical Electronics Engineering from Bahauddin Zakariya University, Multan, and M.Sc. degree in Electrical Engineering with a specialization in Control Systems from the University of Engineering and Technology, Lahore in 2015 and 2018, respectively. His area of research includes power electronics, control systems and electric machines. He is affiliated with academia since 2016 and currently, working as a Lecturer in the NFC Institute of Engineering & Technology, Multan at the department of Electrical Engineering. He is also supervising projects and conducting research funded by the IGNITE-National Funding organization.

Dr. Arslan Ahmed Amin received B.Sc., M.Sc. and Ph.D. degrees in Electrical Engineering with specialization in Control Systems from the University of Engineering and Technology, Lahore. He also holds M.B.A. degree with specialization in 'Management' from Virtual University of Pakistan. He possesses 10 years of relevant industrial and academic experience in Pakistan's reputed organizations. In the industry, he has worked as Professional Electrical & Instrumentation Engineer in the prestigious oil and gas organization, Pakistan Petroleum Limited (PPL) for seven years and served in various domains for installation, maintenance and commissioning of the latest systems such as Electrical Power Network and Distribution, Power Systems Control, PLCs, SCADA, DCS, Process Control, ESD, and Alarm Management Systems. In the academics, he has taught for three semesters in the National Textile University, Faisalabad and was actively involved in the maintenance of the electrical network of the university and conducted energy audit inspections of various local textile mills. He is currently working as Assistant Professor at FAST NUCES Chiniot-Faisalabad Campus and supervising industrial visits of the students for their practical exposure. His research interests include fault-tolerant control systems, control systems' reliability, safety control systems, non-linear control, and control system stability and design..

Neha Masroor did her Bachelor of Science in Electrical Engineering from Pakistan Institute of Engineering and Applied Sciences. Her area of interest includes Renewable Energy Technologies, Sustainable Development, Energy Economics and Econometrics, and Energy Policy. She is currently pursuing her Masters in Energy Systems Engineering from National University of Sciences and Technology, Pakistan.

Huda Mahmood completed her Bachelor of Science in Electrical Engineering from Pakistan Institute of Engineering and Applied Sciences in 2018. With her interest in renewable energy, she chose Power Engineering as her field of further study. She wishes to pursue studies in her field of interest while targeting the development of the renewable power systems through innovative and sustainable methods. Currently, she is working in Pakistan Telecommunications Company Limited as an Assistant Manager.

Muhammad Abubakar received his B.S. degree in Electrical Engineering from University of Engineering and Technology (UET) Lahore and MS degree in Nuclear Engineering from Pakistan Institute of Engineering and Applied Sciences (PIEAS), Pakistan. He is currently a lecturer at Pakistan Institute of Engineering and Applied Sciences (PIEAS), Pakistan. His research interests include Power Drives, Smart grid, Power System Operation, Renewable energy resources, Power System Protection and High Voltage Engineering.